Behavioral and neurochemical studies of inherited manganese-induced dystonia-parkinsonism in *Slc39a14*-knockout mice

Alexander N. Rodichkin[1], **Melissa K. Edler**[2], **Jennifer L. McGlothan**[1], **Tomás R. Guilarte**[1,*]

[1]Brain, Behavior, & the Environment Program, Department of Environmental Health Sciences, Robert Stempel College of Public Health & Social Work, Florida International University, Miami, Florida 33199

[2]Brain Health Research Institute, Kent State University, Kent, Ohio 44242

Abstract

Inherited autosomal recessive mutations of the manganese (Mn) transporter gene *SLC39A14* in humans, results in elevated blood and brain Mn concentrations and childhood-onset dystonia-parkinsonism. The pathophysiology of this disease is unknown, but the nigrostriatal dopaminergic system of the basal ganglia has been implicated. Here, we describe pathophysiological studies in *Slc39a14*-knockout (KO) mice as a preclinical model of dystonia-parkinsonism in *SLC39A14* mutation carriers. Blood and brain metal concentrations in *Slc39a14*-KO mice exhibited a pattern similar to the human disease with highly elevated Mn concentrations. We observed an early-onset backward-walking behavior at postnatal day (PN) 21 which was also noted in PN60 *Slc39a14*-KO mice as well as dystonia-like movements. Locomotor activity and motor coordination were also impaired in *Slc39a14*-KO relative to wildtype (WT) mice. From a neurochemical perspective, striatal dopamine (DA) and metabolite concentrations and their ratio in *Slc39a14*-KO mice did not differ from WT. Striatal tyrosine hydroxylase (TH) immunohistochemistry did not change in *Slc39a14*-KO mice relative to WT. Unbiased stereological cell quantification of TH-positive and Nissl-stained estimated neuron number, neuron density, and soma volume in the substantia nigra pars compacta (SNc) was the same in *Slc39a14*-KO mice as in WT. However, we measured a marked inhibition (85–90%) of potassium-stimulated DA release in the striatum of *Slc39a14*-KO mice relative to WT. Our findings indicate that the dystonia-parkinsonism observed in this genetic animal model of the human disease is associated with a dysfunctional but structurally intact nigrostriatal dopaminergic system. The presynaptic deficit in DA release is unlikely to explain the

totality of the behavioral phenotype and points to the involvement of other neuronal systems and brain regions in the pathophysiology of the disease.

Introduction

Manganese (Mn) is an essential trace element and required cofactor for many enzymes critical for human health [1]. Since the early 1800s, occupational exposure to very high concentrations of Mn has provided evidence that when brain Mn concentrations increase significantly above physiological levels, Mn is neurotoxic and results in a neurological syndrome with early psychiatric symptoms followed by a form of parkinsonism with dystonia that is refractory to levodopa treatment, the pharmacotherapy used to control movement abnormalities in idiopathic Parkinson's disease [2–6].

Historically, Mn-induced neurological disease has been most widely studied in occupationally exposed adult populations [2,3,6]. However, humans are exposed to Mn from a variety of occupational and environmental sources [3–6], and recent cases of Mn-induced parkinsonism have been described in clinical populations. For nearly two decades, several reports have described young adult drug addicts exhibiting parkinsonism with dystonia as a result of injecting high Mn concentrations as a byproduct of the synthesis of the illicit psychostimulant drug ephedron [7–20]. More recently, childhood-onset dystonia-parkinsonism with increased blood and brain Mn concentrations has also been described in individuals with inherited autosomal recessive mutations of the Mn transporter genes *SLC30A10* [21–28] and *SLC39A14* [29–33]. These genetic mutations produce dysfunction of Mn transporters leading to highly elevated Mn concentrations in the blood and brain and clinical expression of childhood-onset dystonia-parkinsonism. One important aspect of this population of Mn transporter mutation carriers is that the chronic Mn exposure occurs when the brain is developing in contrast to adult Mn exposures in the case of occupational and ephedron addicts in which the exposures typically occur when the brain is fully developed. Therefore, it is possible that neuronal systems and brain regions are differentially affected based on the age when the high Mn exposure occurs in the brain.

Nevertheless, the discovery of inherited autosomal recessive mutations of the Mn transporter genes *SLC30A10* and *SLC39A14* has revolutionized the study of Mn homeostasis and neurotoxicity [34]. These genes code for critical Mn transporters that are involved in the efflux (*SLC30A10*) and influx (*SLC39A14*) of Mn in cells to maintain Mn homeostasis. These clinical populations have significantly advanced our understanding of Mn homeostasis and Mn-induced neurological disease in that these Mn transporters work in concert to excrete Mn from the body and disruption of this fine balance results in systemic Mn retention and highly increased concentrations of Mn in the brain [34]. Despite these important findings, there is a paucity of knowledge on the neuronal systems and brain regions affected in the inherited mutation carriers and there is a lack of comprehensive

neuropathological studies in humans with the disease and in preclinical animal models in order to understand the pathophysiology of childhood-onset dystonia-parkinsonism of *SLC39A14* mutation carriers.

While significant research in experimental animal models, and more limited studies in humans, has been described with adult-onset Mn-induced parkinsonism and its effects on the nigrostriatal dopaminergic system [2–6], less is known about the effects of chronically elevated blood and brain Mn concentrations during early life as is the case with individuals expressing the autosomal recessive mutations of the *SLC39A14* and *SLC30A10* genes. However, one of the most consistent changes in brain chemistry with Mn exposure in adult animals is the inhibition of dopamine (DA) release [35–38]. We have previously shown that non-human primates chronically exposed to Mn as young adults with subtle motor function deficits have significant impairment of *in vivo* amphetamine-induced DA release in the caudate/putamen measured using Positron Emission Tomography (PET) [35,36] as well as in the frontal cortex [37]. Similarly, rodents exposed to Mn as adults also have inhibition of potassium-stimulated DA release in the striatum [38]. Therefore, inhibition of striatal DA release whether stimulated by amphetamine or potassium depolarization is a consistent observation on the effects of chronic adult Mn exposure on DAergic circuits in experimental animal models.

The recent availability of *Slc30a10* and *Slc39a14* global knockout (KO) mice provide a genetic-based approach to study Mn-induced neurological dysfunction and underlying neuropathology. Previous studies have shown that *Slc39a14*-KO mice exhibit increased blood and brain Mn concentrations as well as motor function deficits and postural and gait abnormalities as in the human *SLC39A14* mutation carriers [39–41]. Notably, *Slc39a14*-KO mice from a B6:129 hybrid background were backcrossed onto a 129S6/SvEvTac strain, similar blood and brain increases in Mn concentrations were obtained [41] indicating that the deletion of *Slc39a14* results in increased blood and brain Mn concentrations despite the genetic background of the mice and increased brain Mn may be responsible for the behavioral changes observed [41]. However, no study to date has described the neurochemical or neuropathological bases of the Mn-induced dystonia-parkinsonism in mice with genetic deletion of these Mn transporters. In the present work, we used *Slc39a14*-KO mice to assess the behavioral, neurochemical, and neuropathology of the nigrostriatal dopaminergic system resulting from increased brain Mn concentrations in young adult male and female mice. The nigrostriatal dopaminergic system of the basal ganglia was initially selected because it has been implicated in Mn-induced parkinsonism with dystonia [3–5,35,36] and in different dystonia animal models [42–47].

Materials and Methods

Animal husbandry and genotyping:

Animal studies were reviewed and approved by the Florida International University Animal Care and Use Committee, comply with the ARRIVE guidelines, and were carried out in accordance with the National Institutes of Health Guide for the Care and Use of Laboratory Animals. The *Slc39a14*-KO founder mice were generously provided by Dr. Robert J. Cousins from the University of Florida, where the colony was originally described

[48]. Briefly and as described in the original publication [48], Zip14 +/− and Zip14 +/+ founder mice were obtained through a contract with the Mutant Mouse Regional Resource Center at the University of California, Davis. A targeted mutation in Zip14 gene (exons 3–5) was generated in strain 129/SvEvBrd derived embryonic stem cells. The chimeric mice were bred to C57BL/6J albino mice to generate Zip14 +/− mice. Zip14 −/− mice were obtained through further breeding of founder Zip14 +/− mice at the University of Florida [48]. Animals were bred using 1:1 male:female heterozygous mice with litters being weaned at post-natal day (PN) 21. Animals were housed on a 12:12 light:dark cycle with ad-libitum food and water access. The rodent chow used was Advanced Protocol Verified 75 IF irradiated 5V75* diet (Lab diets, Ft. Worth, Texas). ICP-MS analysis of Mn, iron, copper, and zinc of this rodent chow indicated the following concentrations: Mn= 110.5 ± 15.7 μg/g; Iron= 163.1 ± 27.8 μg/g; Copper= 10.7 ± 2.2 μg/g, and Zinc= 79.6 ± 14.5 μg/g. All values are mean ± sem of 5 different samples.

For genotyping, a tail clip was taken immediately after weaning using a pair of sterilized scissors. DNA extraction solution (200 μL) was added to the homogenized tissue samples (QuickExtract DNA Extraction Solution 1.0, Lucigen, Middleton, WI) and heated to 65°C for 6 min and 95°C for 2 minutes. A Verti Applied Biosystems Thermocycler (ThermoFisher Scientific, Waltham, MA) was used for the PCR reaction under the following conditions: 1) – 95°C for 5min, 2) – 95°C for 30sec, 53°C for 30sec and 72°C for 1min for 35 cycles, 3) – 72°C for 10min. The following primer sequences were used: WT forward: 5' – TCA TGG ACC GCT ATG GAA AG – 3'; WT reverse: 5' – GTG TCC AGC GGT ATC AAC AGA GAG – 3'; KO forward: 5' – TGC CTG GCA CAT AGA AAT GC – 3'; KO reverse: 5' – GCA GCG CAT CGC CTT CTA TC – 3'. PCR products were run through 1.5% agarose gel made in 1xTAE buffer containing Gel Red stain (3.75μl of Gel Red in 100ml agarose; Biotum, Fremont, CA) at 120V for 90min with WT band at 164bp and KO band at 469bp. [see example of gel genotyping Supplementary Fig. 1].

Metal analysis:

Brain tissue and whole blood specimens for metals analysis were obtained from animals that were used in behavioral assessments. Tissue metals concentrations were corrected for wet tissue weight.

Blood metals: Whole blood was obtained immediately following decapitations and collected directly into K_2EDTA coated tubes (BD Vacutainer, Becton Dickinson and Company, Franklin Lakes, NJ). 100 μL of whole blood was mixed with 250 μL tetramethylammonium hydroxide (TMAH) solution and allowed to incubate for 10 minutes at room temperature (RT). Afterwards, 50 μL of internal standards (IS) mixture containing lithium, yttrium and germanium was added. A 0.005% EDTA and 0.005% Triton-X solution made in ultrapure water was used to bring the total volume to 5 mL, resulting in final IS concentration of 10 μg/L. The samples were then placed into the autosampler (CETAC-ASX 520, ThermoFisher Scientific, Waltham, MA) and directly injected into the ICP-MS (iCAP-TQ, ThermoFisher Scientific, Waltham, MA) using the S-SQ-KED High Sensitivity detection mode. Qtegra Software (ThermoFisher Scientific, Waltham, MA) was used to construct the calibration curves and perform the analysis [49].

Striatum metals: Striatal punches were taken from flash frozen tissue slabs obtained after euthanizing of mice. Tissue punches were weighed and stored at −80°C until analysis. Samples were mixed with 1 ml of concentrated HNO_3 and allowed to digest for 2 hours at 95°C in a heating block. After digestion, samples were allowed to cool down to room temperature and 100 μL of internal standard (IS) mixture containing lithium, yttrium and germanium was added. Total volume was brought up to 10 ml using 3% HNO_3 made in ultrapure water, resulting in final IS concentration of 10 μg/L. Both blood and brain samples and calibration curve solutions were processed into the autosampler (CETAC-ASX 520, ThermoFisher Scientific, Waltham, MA) and injected into the ICP-MS (iCAP-TQ, ThermoFisher Scientific, Waltham, MA) using S-SQ-KED High Sensitivity detection mode. Qtegra Software (ThermoFisher Scientific, Waltham, MA) was used to construct the calibration curves and perform the analysis.

Behavioral Assessment:

All behavioral tests were performed between 12:00 and 18:00 hr, during the light cycle, with the exception of locomotor activity, that was performed in the dark cycle. Separate naïve animals were used for each test, with 1 male or female animal per litter used for each endpoint.

Activity Cages: For locomotor activity recordings, naive animals were habituated to the behavior room for 30 minutes. Animals were placed into the activity cages (Activity Cages Monitor SOF-812, Med Associates, Fairfax, VT) for 60 minutes. All locomotor activity recordings were performed after 19:00, during the dark cycle.

Rotarod: Rotarod testing took place over the course of 3 days. In the beginning of each day, the animals were habituated to the testing room for 10 minutes. Following the habituation period, they were trained on the rotarod (Columbus Instruments, Columbus, OH) for 5 min at 4RPM and then allowed to rest in their home cage for 30 minutes. After the resting period concluded, animals were placed on the rotarod, starting at 4RPM and accelerating by 4 RPM every 30 seconds, for 3 trials per day. Latency-to-fall was recorded and values from three trials were averaged [50].

Behavioral observations for dystonia features using the tail suspension test: We performed the tail suspension test and observed for dystonia-like features as described in previous studies [46,51,52]. The animal was gently and carefully suspended by the end of the tail 20cm from the bottom of the cage for the duration of 1 minute and recorded on video. A blinded investigator, unfamiliar with the animals analyzed the videos, screening for the following behaviors: front limb clasping, hind limb clasping, truncal torsion, cervical torsion, splaying of the toes, unilateral use of limbs and decreased movement. At PN21, we also observed for torticollis, retrocollis, straub tail, backward walking, foot dragging and splayed paws from videos of *Slc39a14*-KO mice compared to WT. The number of *Slc39a14*-KO mice expressing these abnormal behaviors is provided in supplementary Table 1.

Analysis of dopamine and metabolites concentrations in the corpus striatum:

Tissue punches of the striatum were obtained at the level of the lateral ventricles [AP: 0.14 DV: −3.5 ML: 2.0] from brains of WT and *Slc39a14*-KO mice, and the tissue immediately frozen at −80°C until analysis. On the day of the analysis, sample weights were recorded, the tissue was placed into 30x w/v 0.1M perchloric acid and went through 3 cycles of sonication 10s-on/10s-off (Tekmar Sonic Disruptor, Teledyne Tekmar Company, Inc., Mason, OH) while on ice. The resulting solution was filtered using PTFE-membrane 20 μm centrifugal tubes (Ultrafree-MC Centrifugal Devices, Millipore-Sigma, Burlington, MA) (4°C, 15,000g,15 min). The protein pellet was frozen at −80°C until analysis. The resulting supernatant was diluted in 0.1M perchloric acid at a 1:3 ratio and 10uL were injected into the HPLC-ECD (Dionex Ultimate 3000, ThermoFisher Scientific, Waltham, MA) using the MDTM mobile phase, reverse phase column (C18-Hypersil 150 mm x 2.1 with 3 μm particle size, ThermoFisher Scientific, Waltham, MA) and amperometric cell (Dionex Ultimate 3000 ECD-3000RS Electrochemical Detector, ThermoFisher Scientific, Waltham, MA) set at +400 mV, 10 nA gain with 0.4 mL/min flow rate. 50 ng/ml 2,5-dihydroxybemzoic acid was used as the internal standard [53]. The recovered protein pellets were analyzed using the commercially available BCA assay (Pierce BCA Protein Assay Kit, ThermoFisher Scientific, Waltham, MA). Dopamine and metabolite concentrations were normalized with protein concentrations.

Tyrosine hydroxylase (TH) immunohistochemistry:

Animals were perfused using 4% paraformaldehyde (PFA) solution made in 0.1M phosphate buffer. The extracted tissue was suspended in 4% PFA for 24 hours and cryoprotected in 30% sucrose solution for 48 hours. Snap-frozen brains were sectioned at 40 μm (American Optical Company Microtome, Model 860) with sections placed in individual wells containing freezing storage solution (30% glycerol, 30% ethylene glycol, 30% dH$_2$O and 10% 0.24 M phosphate buffer). Every third section throughout the SNc was stained for TH, the rate-limiting enzyme for DA synthesis, and used for unbiased stereological cell counting. For TH optical density in the striatum, every sixth section was used. The sections were washed in a 1x phosphate-buffer saline solution (PBS, pH 7.4) at room temperature (RT). Antigen retrieval was performed using 10 mM sodium citrate buffer, at 37°C for 30 min which was followed by a 20 min incubation at RT. Endogenous peroxidase was quenched in 2.5% Hydrogen Peroxide (H$_2$O$_2$) made in 75% methanol solution for 20 min at RT. Tissue sections were pre-blocked using 0.6% Triton X-100, 5% bovine serum albumin, and 4% normal horse serum (S-2000, Vector Laboratories, Burlingame, CA) for 1hr at RT. Tissue was incubated in a 1:10,000 primary antibody (MAB-318 Anti-Tyrosine Hydroxylase monoclonal antibody, clone LNC1, Millipore-Sigma, Burlington, MA) overnight at RT. On the following day, the tissue was placed in a biotinylated secondary antibody solution 1:200 (BA-2000, Vector Laboratories, Burlingame, CA), containing 2% normal horse serum for 1hr at RT. The tissue was then incubated for 1 hour at RT in Avidin-biotin-peroxidase complex (ABC kit PK-6100, Vector Laboratories, Burlingame, CA) followed by development in 3,3'-diaminobenzidine for 10 min at RT (DAB kit SK-4100, Vector Laboratories, Burlingame, CA). Sections were mounted on slides, dehydrated in a series of ethanol solutions and cover slipped using the EMS-DPS mounting medium.

Unbiased stereological of TH and Nissl estimated neuron number, neuron density (Nv), and soma volume (SV):

Using the Allen mouse coronal brain atlas (Allen Atlas for Brain Science), we measured TH-positive and Nissl Nv and SV in the SNc of PN60 male and female wildtype (n = 12: 6 male, 6 female) and *Slc39a14*-KO (n =12: 6 male, 6 female) mice. All Nv and SV data were collected using StereoInvestigator software (Version 11.11.2, MBF Bioscience, Williston, VT, RRID:SCR_002526) and an Olympus BX-51 photomicroscope (Olympus, Center Valley, PA) equipped with a digital camera by a single, blinded observer. Initial subsampling techniques were performed to determine appropriate sampling parameters [54]. Beginning at a random starting point, TH-positive and Nissl Nv (mm^3) were obtained using the optical dissector probe at 40x (N.A. 0.75) under Köhler illumination. Six equidistant sections (1:3 series) throughout the SNc were selected for TH Nv quantification, while 3–4 sections were used to collect Nissl Nv (1:6 series). TH-positive and Nissl neurons were designated with a single marker per stain, and sampling area size was 100×100 with a dissector height of 7 μm and a guard zone of 2%. Mounted section thickness was measured every fifth sampling site. Densities were calculated as the population estimate of TH-positive or Nissl-positive markers divided by planimetric volume of the dissector for each area of interest and averaged for every animal [55]. SV was collected for every TH-positive neuron and every fourth Nissl-stained neuron using the isotropic nucleator simultaneously during the optical fractionator probe. Six rays were used to define the soma edge. The average measured thickness for TH-stained sections was 19.49 μm and for Nissl sections was 13.00 μm, and the mean number of sampling sites for TH was 169 ± 39 and for Nissl was 56 ± 5 with a Gunderson coefficient of error (CE) of 0.06. The mean number of nucleators for TH was 121 and for Nissl was 86 with average CEs 0.01 for SV.

In vivo microdialysis and HPLC analysis of dopamine and metabolites in dialysates: *Cannulations:*

Animals were anesthetized with an intraperitoneal injection of ketamine (100 mg/kg) and xylazine (10mg/kg). Once the animals no longer responded to paw pinches and blinking reflexes were not observed, animals were administered atropine (5mg/kg, subcutaneous). A small amount of betadine was used to prepare the incision site. Following betadine application, a 100 μl injection of lidocaine was made in the same location. A presterilized scalpel blade was used to make an incision in the scalp, approximately 2 cm along the sagittal suture, exposing the skull. Following the incision, the mouse was placed into the stereotaxic frame (Neurostar, Tubingen,Germany) and eye ointment was applied. The coordinates for the guide cannula placement (MBR-5 5mm guide cannula, BASi, West Lafayette, IN) were: AP: +1.18, ML: +1.5, and DV: −2.4 [56] and the cannula implant was secured with small anchor screws which were set into the skull (self-tapping bone anchor screws, BASi, West Lafayette, IN). Loctite-444 was used to bind the cannula and screws together with the bone. Upon successful cannulation, animals were administered yohimbine (2 mg/kg) and meloxicam (5 mg/kg) and monitored until voluntary movement appeared. Prior to *in* vivo microdialysis, animals went through a 3-day recovery period with daily administrations of meloxicam (5mg/kg). Workup, cannulations, and recovery were all completed on heating pads.

In vivo microdialysis:

Animals were habituated to the room for 30 minutes. Immediately before the procedure, animals were fitted with collars and the dummy probe was removed from the guide cannula and replaced with the actual probe (MBR 1–5, 1mm probe, BASi, West Lafayette, IN). Animals then were connected to microdialysis tubing and the Raturn system via the collar and artificial CNS fluid (NaCl 147 mmol/L, KCl 2.7 mmol/L, $CaCl_2$ 1.2 mmol/L, $MgCl_2$ 0.85 mmol/L, Harvard Apparatus, Holliston, MA) was perfused for an equilibration period of 3 hours at 1 μl/min. Following the equilibration period, 15 samples in 20-minute intervals were collected at 1 μl/min (BAS Honeycomb refrigerated fraction collector, BASi, West Lafayette, IN) into 300 μl limited volume inserts containing 2 μl of 0.1M perchloric acid, resulting in 22 μl final volume per sample. Immediately after collection, each sample was transferred to the HPLC-ECD system for injection and analysis, using the same parameters as the analysis for striatal dopamine concentrations [53]. Neuronal depolarization in the target region was achieved by switching the perfusion fluid to 120 mM KCl solution (made in aCNS fluid) for a 20-minute per sample period during the 5th sample collection phase. *In vivo*-microdialysis was performed during the night cycle, with pairs of WT and KO animals being sampled at the same time side-by-side with the same solutions. Verification of dialysis probe location in the striatum was performed using Nissl staining and the findings are provided in Supplementary Fig. 2.

Statistical Analysis

Data analysis was performed using unpaired t-tests comparing the means of wildtype versus *Slc39a14*-KO mice. Rotarod data were analyzed using a two-way repeated measures ANOVA. Prior to analyses, data were examined for outliers using the ROUT method (Q = 1). In addition, tests for equality of variance (F-test) and normality of residuals were performed. Statistical analyses were completed using GraphPad PRISM (Version 8.4.0 (455), La Jolla, CA), and α was set at 0.05.

Results

Body and brain weight of wildtype (WT) and *Slc39a14*-KO mice:

Most of the studies were performed in wildtype (WT) and *Slc39a14*-KO mice at postnatal day 60 (PN60). However, body weights were recorded at PN30, PN45, and PN60 (Supplementary Fig. 3). Analysis of variance indicates that there was no significant effect of genotype on body weight of male ($F_{1,15}$= 0.910, p=0.36) or female mice ($F_{1,15}$= 0.286, p=0.60). At PN60, when animals were euthanized, whole brain weight (frozen) was measured with no significant effect of genotype in male and female mice brain weight (Supplementary Fig. 3).

Blood and brain metals concentrations:

We measured the concentrations of Mn, copper, iron, and zinc in whole blood samples from WT and *Slc39a14*-KO male and female mice at PN60. Highly significant increases in blood Mn concentrations were found in both male (Fig. 1A) and female (Fig. 1B) *Slc39a14*-KO mice relative to WT. On the other hand, no differences were identified in iron, copper, or

zinc concentrations in the blood of male (Fig. 1A) or female (Fig. 1B) *Slc39a14*-KO relative to WT at this age. This is consistent with what was found in the *SLC39A14* mutation carriers [29]. We also measured metal concentrations in the striatum, as this brain region is associated with movement abnormalities and is implicated in dystonia-parkinsonism. Figure 1 shows that Mn concentrations in the striatum of PN60 *Slc39a14*-KO was approximately 5 times higher than WT in both male (Fig. 1C) and female (Fig. 1D) mice. No significant effect was determined for genotype on iron, copper, or zinc concentrations in the striatum of male (Fig. 1C) or female (Fig. 1D) mice at this age.

Behavioral studies:

To assess the effect of the *Slc39a14* deletion on locomotor activity, motor coordination, and dystonia-like movements, we performed a variety of behavioral and observational studies on male and female PN21 (weaning) and PN60 mice.

Locomotor activity: Locomotor activity was assessed during the dark cycle using automated activity cages at PN60. Significant impairment of locomotor activity was demonstrated in both male (Fig. 2B) and female (Fig. 2C) *Slc39a14*-KO mice relative to WT. Male (Fig. 2B) and female (Fig. 2C) PN60 *Slc39a14*-KO mice had significantly decreased distance travelled, speed, and vertical counts (rearing), with an increase in resting time, consistent with a significant impairment in locomotor behavior.

Rotarod measurements: Rotarod analysis examined the effect of global *Slc39a14* deletion and resulting increased brain Mn concentrations on motor coordination and motor skill learning. Both male (Fig. 2D) and female (Fig. 2E) *Slc39a14*-KO mice experienced a significant impairment relative to WT. For example, the latency to fall from the turning rod decreased for all 3 days in *Slc39a14*-KO mice compared to WT. Combined, the locomotor and rotarod results clearly indicate significant impairment of normal motor function and coordination in the PN60 *Slc39a14*-KO male and female mice relative to WT.

Observational studies of dystonia-like movements and ataxia (video and pictures): We observed abnormal locomotor behavior in some of the *Slc39a14*-KO mice at weaning (PN21). That is, *Slc39a14*-KO mice express backward walking behavior (see Supplementary Movie 1) at weaning with a wider separation of the hindlimbs and a shuffling gait. To our knowledge, this type of backward walking behavior has only been previously observed in moonwalker mice [57]. Further, when *Slc39a14*-KO mice attempted to move forward, dragging of the hindlimb was noted in some animals (see Supplementary Movie 2). The backwards movement in the *Slc39a14*-KO was also observed in *Slc39a14*-KO mice at PN60. A portion of *Slc39a14*-KO mice had tilting of the head to the left side (torticollis) and back (retrocollis), and straub tail (Supplementary Table 1). Using the tail suspension test, we showed that *Slc39a14*-KO mice expressed dystonia-like movements such as trunk twisting and hindlimb clasping a greater percentage of the time than WT (Fig. 2F and Supplementary Table 1).

Neurochemical and neuropathological assessment of nigrostriatal dopaminergic system:

The motor function deficits of the *Slc39a14*-KO mice could be the result of dysfunction or degeneration of the nigrostriatal dopaminergic system as dopaminergic (DA) neurons of the substantia nigra pars compacta (SNc) have been implicated in a variety of movement disorders including dystonia and parkinsonism with idiopathic Parkinson's disease being the most prominent form of parkinsonism. Therefore, we performed an assessment of nigrostriatal dopaminergic markers in PN60 WT and *Slc39a14*-KO mice.

Analysis of dopamine and metabolite concentrations in the striatum: We performed HPLC-electrochemical detection of DA and its metabolites 3,4-dihydroxyphenylacetic acid (DOPAC) and homovanillic acid (HVA) as well as metabolite to DA ratios in the striatum of male and female WT and *Slc39a14*-KO mice at PN60. Global deletion of the *Slc39a14* gene which produces increased blood and brain Mn concentrations and motor function deficits had no significant effect on striatal DA concentrations or in the concentrations of the DA metabolites DOPAC or HVA in male (Fig. 3A) or female (Fig. 3B) *Slc39a14*-KO mice compared to WT. Furthermore, the ratios of DOPAC/DA and HVA/DA which are measures of DA turnover also were not significantly affected in *Slc39a14*-KO mice of either sex (Fig. 3A-B).

Tyrosine hydroxylase (TH) immunohistochemistry and optical density analysis of nigrostriatal dopaminergic neuron terminals in the striatum: To determine if there was an effect on nigrostriatal dopaminergic terminals in the striatum, we performed TH immunohistochemistry in the striatum of WT and *Slc39a14*-KO mice. Optical density measures demonstrated no differences in the level of TH immunoreactivity by genotype (Fig. 3C-E). These findings indicate that nigrostriatal dopaminergic terminals in the striatum of *Slc39a14*-KO mice are intact, despite highly increased brain Mn concentrations and deficits in motor function.

TH-positive and Nissl-stained neuron density (Nv) and soma volume (SV) in the SNc: To further assess the integrity of nigrostriatal DAergic neurons, we performed unbiased stereological quantification of TH-positive Nv and SV in the SNc. TH-positive Nv and Sv did not differ in the SNc of WT and *Slc39a14*-KO male (Fig. 4A, 4C) and female (Fig. 4B, 4D) mice. To confirm the lack of an effect resulting from the *Slc39a14* gene deletion on overall Nv and Sv, we also analyzed Nissl Nv an Sv in the SNc. Consistent with the TH-positive Nv and SV, there were no differences in Nissl Nv or Sv between *Slc39a14*-KO mice and WT male or female mice (Supplementary Fig. 4). In order to obtain Nv, for either TH-positive or Nissl-stained neurons in the SNc, the average estimated number of neurons is divided by the average planimetric volume. Analysis of the average estimated number of TH-positive or Nissl-stained neurons also shows no significant differences between WT and *Slc39a14*-KO mice of either sex (Supplementary Table 2).

***In vivo* microdialysis of basal and potassium-stimulated dopamine release in the striatum:** Previous work from our laboratory on the effects of chronic Mn exposure in young adult non-human primates showed that a prominent effect of chronic Mn exposure on the nigrostriatal dopaminergic system was marked inhibition of amphetamine-induced

DA release in the caudate/putamen (striatum) measured by Positron Emission Tomography [35,36]. This effect of chronic Mn exposure has also been shown in adult mice chronically exposed to Mn [38]. In this rodent study, striatal DA release was stimulated using high potassium concentrations. Therefore, we measured the basal and potassium-stimulated release of DA in the striatum using *in vivo* microdialysis. We found a marked inhibition (85–90%) of potassium-stimulated DA release in PN60 *Slc39a14*-KO male (Fig. 5C) and female (Fig. 5D) mice relative to WT consistent with previous Mn-exposed non-human primate [35,36] and in rodents [38].

Discussion

To our knowledge, this is the first report describing neurochemical changes of the nigrostriatal dopaminergic system associated with the motor function deficits, postural and gait abnormalities in *Slc39a14*-KO mice, a preclinical model of the childhood-onset dystonia-parkinsonism resulting from the inherited autosomal recessive mutations of the *SLC39A14* gene in humans. As outlined by Tuschl et al., [29] in their original communication describing individuals expressing this inherited mutation, there are similarities in the behavioral deficits in *Slc39a14*-KO mice as in the human disease. For instance, affected individuals experience an early loss of developmental milestones, progressive dystonia, and bulbar dysfunction. They later develop severe generalized and pharmaco-resistant dystonia, spasticity, scoliosis, and loss of independent ambulation. In some cases, there was parkinsonism with hypomimia, tremor, and bradykinesia. From a neuroimaging perspective, the *SLC39A14* mutation carriers exhibited hyperintensive signals based on T1-weighted magnetic resonance imaging (MRI) of the brain consistent with the known regional brain deposition that occurs with increased Mn exposure [29].

In the present work, *Slc39a14*-KO mice express motor function deficits and dystonia-like movement with elevated blood and brain Mn concentrations similar to humans carrying the *SLC39A14* mutation (Fig. 1 and Fig. 2). An early onset dystonia was expressed in the form of trunk twisting, and hindlimb clasping that appeared at PN21 and remained in PN60 *Slc39a14*-KO mice. Importantly, at PN21, some of the *Slc39a14*-KO mice (see Supplementary Movie 1) exhibited backward walking similar to moonwalker mice [57]. The moonwalker mice are a model of inherited cerebellar ataxia resulting from a gain-of-function mutation in the gene encoding the cation-permeable transient receptor potential channel (TRPC3) [57]. Further, *Slc39a14*-KO mice expressed torticollis and straub tail as described in previous studies [39–41]. It has been suggested that these postural abnormalities could affect behavioral performance of the *Slc39a14*-KO mice [58]. However, a recent study has shown that *Slc39a14*-KO mice with torticollis and/or straub tail, had deficits in behavioral test scores similar to *Slc39a14*-KO mice that did not display these postural abnormalities [59]. Therefore, the postural abnormalities do not interfere with the accurate assessment of motor function deficits in *Slc39a14*-KO mice.

The *Slc39a14*-KO mice used in this study also express deficits in other motor function test as it was noted in the original manuscript that first described the *Slc39a14*-KO mice used in the present study. In their work, the authors showed significant impairment in the balance beam, pole descent test, and forelimb activity [39] at a similar age (PN60) and in

older (up to PN120) *Slc39a14*-KO mice than in the present study. Other studies assessing the behavioral phenotype of *Slc39a14*-KO mice also showed motor function deficits and postural abnormalities with dystonia-like movements [40,41] consistent with our current findings.

The dystonia-parkinsonism resulting from high brain Mn concentrations in human subjects carrying the inherited *SLC39A14* mutation is thought to involve the basal ganglia, due to their role in motor function, but until now no studies have investigated the neurochemical or neuropathological changes responsible for this clinical phenotype. In the present study, we examined the nigrostriatal dopaminergic system because of its important role in motor function. In addition, the main neuropathology in idiopathic Parkinson's disease is the loss of DA and DA terminals in the striatum and DA cell bodies in the SNc [3–6]. We found that *Slc39a14*-KO mice had normal levels of striatal DA and metabolites as well as their ratios relative to WT (Fig. 3). Furthermore, analysis of DAergic terminals in the striatum using TH immunohistochemistry did not show any difference between *Slc39a14*-KO and WT mice and this was supported by unbiased stereological counting of TH-positive and Nissl-stained neurons in the SNc (Fig. 4 and supplementary Fig. 4). The results showed no differences in DA neuron density or soma volume in the SNc of *Slc39a14*-KO mice relative to WT (Fig. 4 and Supplementary Fig. 4). Furthermore, the estimated number of TH-positive and Nissl-stained neurons in the SNc was not different between *Slc39a14*-KO and WT mice (Supplementary Table 2). Finally, *in vivo* microdialysis in the striatum of *Slc39a14*-KO and WT mice performed at the same time in pairs under the same experimental conditions, did show a marked inhibition (85–90%) of potassium-stimulated DA release in *Slc39a14*-KO mice (Fig. 5). This finding is consistent with previous studies from our laboratory in which we found marked inhibition of amphetamine-stimulated DA release in the caudate/putamen of non-human primates chronically exposed to Mn using Positron Emission Tomography (PET) [35,36] and in Mn-exposed adult mice [38].

The molecular and cellular mechanism(s) of Mn-induced inhibition of DA release is currently not known. However, recent studies using primary neuronal cultures indicate that Mn disrupts SNARE-protein complex vesicle fusion [60], an effect that could be mediated via a Mn-induced overexpression of α-synuclein [61]. These findings indicate that the behavioral phenotype described in *Slc39a14*-KO mice is due, at least in part, to presynaptic function deficits in the form of marked inhibition of DA release with no change in DA or metabolite concentrations in the striatum. Importantly, nigrostriatal DAergic terminals and DA neuron number, density, and soma volume in the SNc were not affected in *Slc39a14*-KO mice relative to WT (Fig. 3, Fig. 4 and Supplementary Fig. 4; Supplementary Table 2). While detailed neuropathological studies of DAergic neurons in the SNc of *SLC39A14* mutation carriers are lacking, a case report of an ephedrone addict has recently been described [62]. In this case report, they show that in the brain of a 33-year-old female ephedrone addict with increased brain Mn and a history of levodopa unresponsive parkinsonism with dysarthria, dystonia, postural instability, cock-gait, and frequent falls, exhibited normal TH-positive staining in DAergic neurons in the SNc [62] consistent with our current results. However, unlike our present study, this case report did not quantify DA neuron number in the SNc.

Our present study provides direct evidence of a dysfunctional but structurally intact nigrostriatal DAergic system in *Slc39a14*-KO mice that exhibited elevated brain Mn concentrations and motor function deficits, dystonia-like movements, and postural abnormalities. This is consistent with the clinical data from Tuschl et al [29] indicating that subjects with the inherited *SLC39A14* mutation do not respond to levodopa therapy [supplementary note 1 in 29]. Our present finding of marked inhibition of DA release in the striatum with no change in DA concentrations or DA neuron degeneration is similar to a mouse model of *DYT1* dystonia [45]. *DYT1* dystonia or early onset torsion dystonia is the most common form of hereditary primary dystonia caused by a mutation in the *TOR1* gene which codes for the torsin A protein. In this dystonia mouse model, the genetic mutation did not affect striatal DA concentrations but produced a marked inhibition of amphetamine-induced DA release in the striatum [42]. Inhibition of DA release in the striatum has also been described in other animal models of dystonia [42–47].

While it is clear that *Slc39a14*-KO mice expressed marked inhibition of DA release, it is not clear which of the motor function changes, dystonia-like movements, and postural and gait abnormalities are associated with this neurochemical deficit. Future rescue studies are likely to provide an answer to this important question. Although in this communication we found no neurodegeneration of TH-positive DAergic neurons in the SNc, it is possible that neurodegeneration is occurring in other brain regions as suggested in the original Tuschl et al., report [29]. That is, they show evidence of neuronal loss in the globus pallidus and dentate nucleus of the cerebellum as well as cortical and cerebellar atrophy in one *SLC39A14* inherited mutation carrier [29]. As some *Slc39a14*-KO mice at weaning (PN21) exhibited backward walking with spreading of the hind limbs resembling the same deficit in moonwalker mice [57], this finding also suggests cerebellar involvement in the pathophysiology of *Slc39a14*-KO mice. Further, evidence of cerebellar involvement exists in other genetic animal models of dystonia and in the human disease [63,64]. Future studies will examine these possibilities in *Slc39a14*-KO mice. While Mn-induced neurological disease was first described nearly two centuries ago [2,3,6], the precise molecular and cellular mechanism(s) and underlying neuropathology are less well-defined. Therefore, *Slc39a14*-KO mice, as well as *Slc30a10*-KO mice, will facilitate additional discoveries on the pathophysiology of Mn neurotoxicity with significant translational implications for the development of effective therapeutic strategies. Finally, although it is highly likely that the behavioral and neurochemical effects that we observed in the present work are the result of the highly elevated brain Mn concentrations, it is possible that there are Mn-independent effects resulting from the loss of the *Slc39a14* gene. Rescue experiments in which brain Mn accumulation are prevented in *Slc39a14*-KO mice are important to determine whether the loss of *Slc39a14* gene expression has any independent effects on the behavioral or neurochemical changes described in this communication.

Supplementary Material

Refer to Web version on PubMed Central for supplementary material.

Acknowledgements

References

1. Aschner JL, Aschner M, Nutritional aspects of manganese homeostasis. Mol. Aspects Med. 26, 353–362 (2005). DOI: 10.1016/j.mam.2005.07.003 [PubMed: 16099026]

2. Couper J, On the effects of the black oxide of manganese when inhaled in the lungs. Brit. Ann. Med. Pharmacol. 1, 41–42 (1837).

3. Guilarte TR, Manganese and Parkinson's disease: a critical review and new findings. Environ. Health Perspect. 118, 1071–1080 (2010). DOI: 10.1590/s1413-81232011001200028 [PubMed: 20403794]

4. Guilarte TR, Manganese neurotoxicity: new perspectives from behavioral, neuroimaging and neuropathological studies in humans and non-human primates. Front. Aging Neurosci. 5, 1–10 (2013). DOI: 10.3389/fnagi.2013.00023 [PubMed: 23430962]

5. Guilarte TR, Gonzales KK, Manganese-induced parkinsonism is not idiopathic Parkinson's disease: Environmental and Genetic Evidence. Toxicol. Sci. 146, 204–212 (2015). DOI: 10.1093/toxsci/kfv099 [PubMed: 26220508]

6. Blanc PD, The early history of manganese and its recognition of its neurotoxicity. NeuroToxicol. 64, 5–11 (2018). DOI: 10.1016/j.neuro.2017.04.006

7. Meral H, Kutukcu Y, Atcama B, Ozer F, Hamamcioglu K, Parkinsonism caused by chronic usage of intravenous potassium permanganate. Neurologist13, 92–94 (2007). DOI: 10.1097/01.nrl.0000253089.20746.a8 [PubMed: 17351530]

8. de Bie RM, Gladstone RM, Strafella AP, Ko JH, Lang AE, Manganese-induced parkinsonism associated with methcathinone (ephedrone) abuse. Arch. Neurol. 64, 886–889 (2007). DOI: 10.1001/archneur.64.6.886 [PubMed: 17562938]

9. Sanotsky Y, et al., Manganic encephalopathy due to "ephedrone" abuse. Mov. Disord. 22, 1337–1343 (2007). DOI: 10.1002/mds.21378 [PubMed: 17566121]

10. Sikk K, et al., Irreversible motor impairment in young addicts-ephedrone, manganism or both? Acta Neurol. Scand. 115, 385–389 (2007). DOI: 10.1111/j.1600-0404.2007.00818.x [PubMed: 17511846]

11. Selikhova M, et al., Parkinsonism and dystonia caused by illicit use of ephedrone-a longitudinal study. Mov. Disord. 23, 2224–2231 (2008). DOI: 10.1002/mds.22290 [PubMed: 18785245]

12. Stepens A, et al., A parkinsonian syndrome in methcathinone users and the role of manganese. New Engl. J. Med. 358, 1009–1017 (2008). DOI: 10.1056/NEJMoa072488 [PubMed: 18322282]

13. Colosimo C, Guidi M, Parkinsonism due to ephedrone neurotoxicity: a case report. Eur. J. Neurol. 16, e114–e115 (2009). DOI: 10.1111/j.1468-1331.2009.02606.x [PubMed: 19453409]

14. Yildirim EA, et al., Chronic manganese intoxication due to methcathinone (ephedron) abuse: a case report. Turk. J. Psychiat. 20, 294–298 (2009).

15. Iqbal M, Monaghan T, Redmond J, Manganese toxicity and ephedrone abuse manifesting as parkinsonism: a case report. J. Med. Case Rep. 6, 52 (2012). DOI: 10.1186/1752-1947-6-52 [PubMed: 22313512]

16. Fudalej S, Kolodziejczyk I, Gajda T, Majkowska-Zwolinska B, Wojnar M, Manganese-induced parkinsonism among ephedron users and drug policy in Poland. J. Addict. Med. 7, 302–303 (2013). DOI: 10.1097/ADM.0b013e3182915dce [PubMed: 23609215]

17. Sikk K, et al., Manganese-induced parkinsonism in methcathinone abusers: biomarkers of exposure and follow-up. Eur. J. Neurol. 20, 915–920 (2013). DOI: 10.1111/ene.12088 [PubMed: 23347399]

18. Poniatowska R, et al., MRI brain findings in ephedrine encephalopathy associated with manganese abuse: single-center perspective. Pol. J. Radiology79, 150–155 (2014). DOI: 10.12659/PJR.889690

Author Manuscript

Author Manuscript

Author Manuscript

Author Manuscript

19. Janocha-Litwin J, Marianska K, Serafinska S, Simon K, Manganese encephalopathy among ephedron abusers-case reports. J. Neuroimaging25, 832–835 (2015). DOI: 10.1111/jon.12173 [PubMed: 25255816]

20. Sikk K, et al., Clinical, neuroimaging, and neurophysiological features of addicts with manganese-ephedrone exposure. Acta Neurol. Scand. 121, 237–243 (2010). DOI: 10.1111/j.1600-0404.2009.01189.x [PubMed: 20028341]

21. Gospe SM, et al., Paraparesis, hypermanganesaemia, and polycythaemia: a novel presentation of cirrhosis. Arch. Dis. Child. 83, 439–442 (2000). DOI: 10.1136/adc.83.5.439 [PubMed: 11040156]

22. Sahni V, et al., Case report: a metabolic disorder presenting a pediatric manganism. Environ. Health Persp. 115, 1776–1779 (2007). DOI: 10.1289/ehp.10421

23. Tuschl K, et al., Hepatic cirrhosis, dystonia, polycythemia, and hypermanganesemia-a new metabolic disorder. J. Inherit. Metab. Dis. 31, 151–163 (2008). DOI: 10.1007/s10545-008-0813-1 [PubMed: 18392750]

24. Brna P, Gordon K, Dooley JM, Price V, Manganese toxicity in a child with iron deficiency and polycythemia. J. Child Neurol. 26, 891–894 (2011). DOI: 10.1177/0883073810393962 [PubMed: 21596707]

25. Quadri M, et al., Mutations in *SLC30A10* cause parkinsonism and dystonia with hypermanganesemia, polycythemia, and chronic liver disease. Am. J. Hum. Genet. 90, 467–477 (2012). DOI: 10.1016/j.ajhg.2012.01.017 [PubMed: 22341971]

26. Stamelou M, et al., Dystonia with brain manganese accumulation resulting from *SLC30A10* mutations: a new treatable disorder. Mov. Disord. 27, 1317–1322 (2012). DOI: 10.1002/mds.25138 [PubMed: 22926781]

27. Tuschl K, et al., Syndrome of hepatic cirrhosis, dystonia, polycythemia, and hypermanganesemia caused by mutations in *SLC30A10*, a manganese transporter in man. Am. J. Hum. Genet. 90, 457–466 (2012). DOI: 10.1016/j.ajhg.2016.07.015 [PubMed: 22341972]

28. Lechpammer M, et al., Pathology of inherited manganese transporter deficiency. Ann. Neurol. 75, 608–612 (2014). DOI: 10.1002/ana.24131 [PubMed: 24599576]

29. Tuschl K, et al., Mutations in *SLC31A14* disrupt manganese homeostasis and cause childhood-onset parkinsonism-dystonia. Nat. Commun. 7, 11601 (2016). DOI: 10.1038/ncomms11601 [PubMed: 27231142]

30. Juneja M, et al., A novel mutation in SLC39A14 causing hypermanganesemia associated with infantile onset dystonia. J. Genet. Med. 20, e3012 (2018). DOI: 10.1002/jgm.3012

31. Marti-Sanchez L, et al., Hypermanganesemia due to mutations in *SLC39A14*: further insights into Mn deposition in the central nervous system. Orphanet J. Rare Dis. 13, 28 (2018). DOI: 10.1186/s13023-018-0758-x [PubMed: 29382362]

32. Rodan LH, et al., Novel founder intronic variant in SLC39A14 in two families causing manganism and potential treatment strategies. Mol. Genet. Metab. 124, 161–167 (2018). DOI: 10.1016/j.ymgme.2018.04.002 [PubMed: 29685658]

33. Zeglam A, Abugrara A, Kabuka M, Autosomal-recessive iron deficiency anemia, dystonia, and hypermanganesemia caused by a new variant mutation of the manganese transporter gene SLC39A14. Acta Neurol. Belg. 119, 379–384 (2019). DOI: 10.1007/s13760-018-1024-7 [PubMed: 30232769]

34. Mukhopadhyay S, Familial manganese-induced neurotoxicity due to mutations in *SLC30A10* and *SLC39A14*. NeuroToxicol. 64, 278–283 (2018). DOI: 10.1016/j.neuro.2017.07.030

35. Guilarte TR, et al., Nigrostriatal dopamine system dysfunction and subtle motor deficits in manganese-exposed non-human primates. Exp. Neurol. 202, 381–390 (2006). DOI: 10.1016/j.expneurol.2006.06.015 [PubMed: 16925997]

36. Guilarte TR, et al., Impairment of nigrostriatal dopamine neurotransmission by manganese is mediated by pre-synaptic mechanism(s): implications to manganese-induced parkinsonism. J. Neurochem. 107, 1236–1247 (2008). DOI: 10.1111/j.1471-4159.2008.05695.x [PubMed: 18808452]

37. Guilarte TR, et al., PET imaging of dopamine release in the frontal cortex of manganese-exposed non-human primates. J. Neurochem. 150, 188–201 (2019). DOI: 10.1111/jnc.14681 [PubMed: 30720866]

38. Khalid M, Aoun AR, Mathews AT, Altered striatal dopamine release following a sub-acute exposure to manganese. J. Neurosci. Methods202, 182–191 (2011). DOI: 10.1016/j.jneumeth.2011.06.019 [PubMed: 21740928]

39. Aydemir TB, et al., Metal transporter Zip14 (Slc39a14) deletion in mice increases manganese deposition and produces neurotoxic signatures and diminished motor activity. J. Neurosci. 37, 5996–6006 (2017). DOI: 10.1523/JNEUROSCI.0285-17.2017 [PubMed: 28536273]

40. Xin Y, et al., Manganese transporter Slc39a14 deficiency revealed its key role in maintaining manganese homeostasis in mice. Cell Disc. 3, 17025 (2017). DOI: 10.1038/celldisc.2017.25

41. Jenkitkasemwong S, et al., SLC39A14 deficiency alters manganese homeostasis and excretion resulting in brain manganese accumulation and motor deficits in mice. Proc. Nat. Acad. Sci. 115, E1769–E1778 (2018). DOI: 10.1073/pnas.1720739115 [PubMed: 29437953]

42. Balcioglu A, et al., Dopamine release is impaired in a mouse model of DYT1 dystonia. J. Neurochem. 102, 783–788 (2007). DOI: 10.1111/j.1471-4159.2007.04590.x [PubMed: 17550429]

43. Hewett J, Johanson P, Sharma N, Standaert D, Balcioglu A, Function of dopamine transporter is compromised in DYT1 transgenic animal model in vivo. J. Neurochem. 113, 228–235 (2010). DOI: 10.1111/j.1471-4159.2010.06590.x [PubMed: 20132487]

44. Song C-H, Fan X, Exeter CJ, Hess EJ, Jinnah HA, Functional analysis of dopaminergic systems in a DYT1 knock-in mouse model of dystonia. Neurobiol. Dis. 48, 66–78 (2012). DOI: 10.1016/j.nbd.2012.05.009 [PubMed: 22659308]

45. Ip CW, et al., Tor1a+/− mice develop dystonia-like movements via a striatal dopaminergic dysregulation triggered by peripheral nerve injury. Acta Neruopathol. Commun. 4, 108. DOI: 10.1186/s40478-016-0375-7

46. Eskow Jaunarajs KL, Scarduzio M, Ehrlich ME, McMahon LL, Standaert DG, Diverse mechanisms lead to common dysfunction of striatal cholinergic interneurons in distinct genetic mouse models of dystonia. J. Neurosci. 39, 7195–7205 (2019). DOI: 10.1523/JNEUROSCI.0407-19.2019 [PubMed: 31320448]

47. Rauschenberger L, et al., Striatal dopaminergic dysregulation and dystonia-like movements induced by sensorimotor stress in a pharmacological mouse model of rapid-onset dystonia-parkinsonism. Exp. Neurol. 323, 113109 (2020). DOI: 10.1016/j.expneurol.2019.113109 [PubMed: 31712125]

48. Aydemir TB, Sitren HS, Cousins RJ, The zinc transporter ZIP14 influences c-Met phosphorylation and hepatocyte proliferation during liver regeneration in mice. Gastroenterology142, 1536–1546.e5. (2012). DOI: 10.1053/j.gastro.2012.02.046 [PubMed: 22374166]

49. Nunes JA, et al., A simple method based on ICP-MS for estimation of background levels of arsenic, cadmium, copper, manganese, nickel, lead, and selenium in blood of the Brazilian population. J. Toxicol. Environ. Health A73, 878–887 (2010). DOI: 10.1080/15287391003744807 [PubMed: 20563921]

50. Loth MK, et al., TSPO in a murine model of Sandhoff disease: presymptomatic marker of neurodegeneration and disease pathophysiology. Neurobiol. Dis. 85, 174–186 (2016). DOI: 10.1016/j.nbd.2015.11.001 [PubMed: 26545928]

51. Liang C-C, Tanabe LM, Jou S, Chi F, Dauer WT, Torsin A hypofunction causes abnormal twisting movements and sensorimotor circuit neurodegeneration. J. Clin. Invest. 124, 3080–3092 (2014). DOI: 10.1172/JCI72830 [PubMed: 24937429]

52. Xiao R, et al., Abnormal cerebellar development is involved in dystonia-like behaviors and motor dysfunction of autistic BTBR mice. Front. Cell Dev. Biol. 8, 231 (2020). DOI: 10.3389/fcell.2020.00231 [PubMed: 32318573]

53. Yang L, Beal MF, Determination of neurotransmitter levels in models of Parkinson's disease by HPLC-ECD. Methods in Mol. Biol. 793, 401–415 (2011). DOI: 10.1007/978-1-61779-328-8_27 [PubMed: 21913116]

54. Slomianka L, West MJ, Estimators of the precision of stereological estimates: An example based on the CA1 pyramidal cell layer of rats. Neuroscience136, 757–767 (2005). DOI: 10.1016/j.neuroscience.2005.06.086 [PubMed: 16344149]

55. Sherwood CC, Raghanti MA, Wenstrup JJ, Is humanlike cytoarchitectural asymmetry present in another species with complex social vocalization? A stereologic analysis of mustached bat

auditory cortex. Brain Res. 1045, 164–174 (2005). DOI: 10.1016/j.brainres.2005.03.023 [PubMed: 15910775]

56. Paxinos G, Franklin KB, The Mouse Brain: In Stereotaxic Coordinates, 2nd edition. (Academic Press, 2001).nd

57. Becker EBE, et al., A point mutation in TRPC3 causes abnormal Purkinje cell development and cerebellar ataxia in moonwalker mice. Proc. Nat. Acad. Sci. 106, 6706–6711 (2009). DOI: 10.1073/pnas.0810599106 [PubMed: 19351902]

58. Taylor CA, et al., Maintaining translational relevance in animal models of manganese neurotoxicity. J. Nutrition150, 1360–1369 (2020). DOI: 10.1093/jn/nxaa066 [PubMed: 32211802]

59. Giraldo G, Janus C, Phenotypic evaluation of a childhood-onset parkinsonism-dystonia mouse model with inherent postural abnormalities. Brain Res. Bull. 166, 54–63 (2021). DOI: 10.1016/j.brainresbull.2020.10.018 [PubMed: 33147520]

60. Wang C, et al., Manganese exposure disrupts SNARE-protein complex-mediated vesicle fusion in primary cultured neurons. Env. Toxicol. 32, 705–716 (2016). DOI: 10.1002/tox.22272 [PubMed: 27125645]

61. Wang C, et al., Alpha-synuclein and calpains disrupts SNARE-mediated synaptic vesicle fusion during manganese exposure in SH-SY5Y cells. Cells7, 258 (2018). DOI: 10.3390/cells7120258

62. Sanotsky Y, et al., Neuropathological findings in ephedrone encephalopathy. Mov. Disord. 35, 1858–1863 (2020). DOI: 10.1002/mds.28125 [PubMed: 32542919]

63. Shakkottai VG, et al., Current opinions and areas of consensus on the role of the cerebellum in dystonia. Cerebellum16, 577–594 (2017). DOI: 10.1007/s12311-016-0825-6 [PubMed: 27734238]

64. Tewari A, Fremoni R, Khodakhash K, It's not just the basal ganglia: cerebellum as a target for dystonia therapeutics. Mov. Disord. 32, 1537–1454 (2017). DOI: 10.1002/mds.27123 [PubMed: 28843013]

Highlights

- *Slc39a14*-KO mice exhibit highly elevated blood and brain manganese concentrations.

- *Slc39a14*-KO mice have significant motor function impairment and early onset dystonia-like movements.

- Analysis of dopamine release shows a marked inhibition in the striatum of *Slc39a14-KO* mice.

- Striatal dopamine levels and nigrostriatal dopaminergic neuron numbers are unchanged in *Slc39a14*-KO mice.

- These studies show that Slc39a14-KO mice replicate many key features of the human disease.
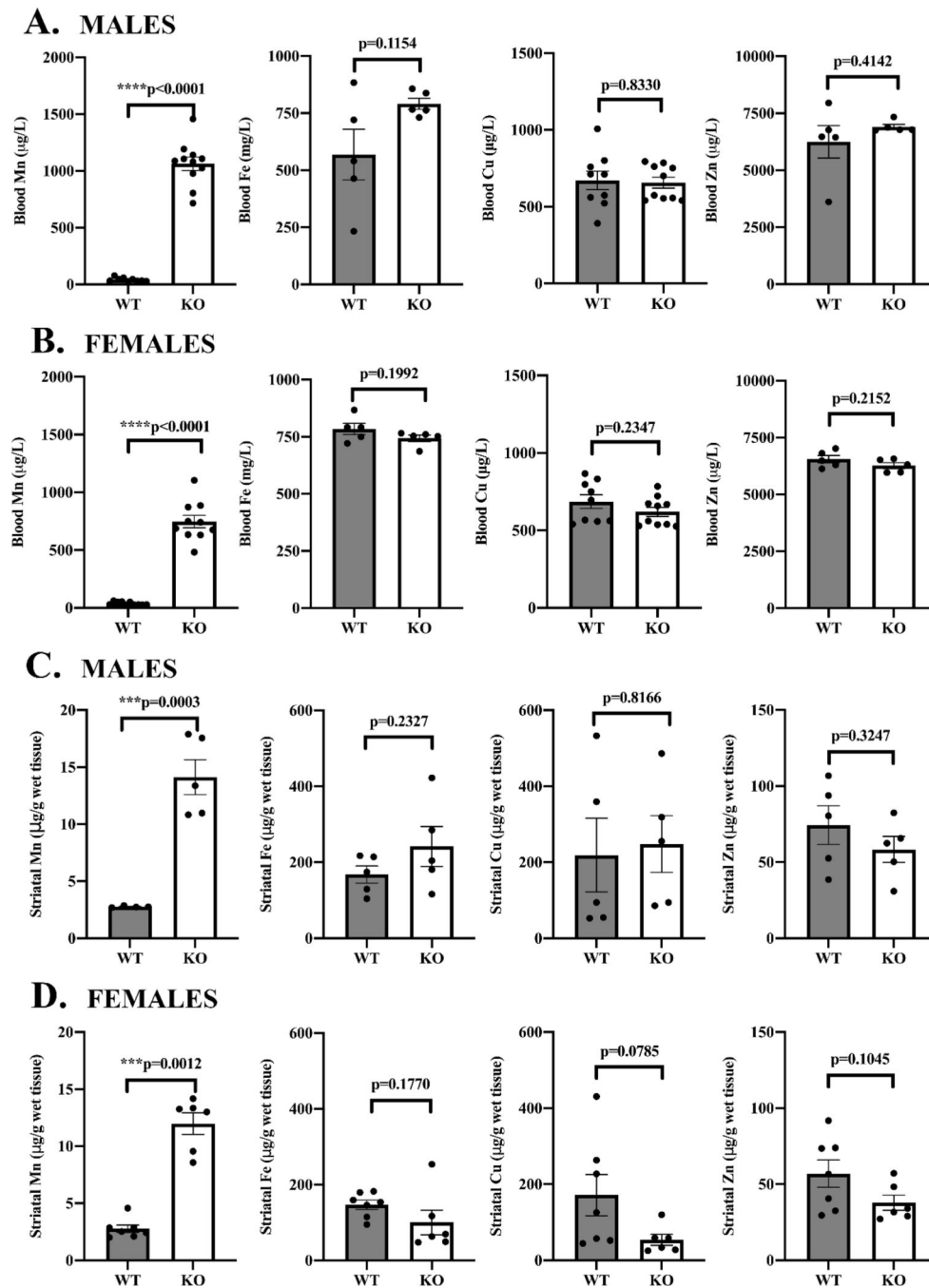
Fig. 1: Blood and brain metals concentrations in WT and *Slc39a14*-KO PN60 mice:
A) Whole blood concentrations of manganese, iron, copper, and zinc in male WT and
KO mice. *Slc39a14*-KO mice exhibited highly significant (p < 0.0001) increases on
blood Mn levels with no effect on other metals concentrations. (n=5–11) B) Similarly,
female *Slc39a14*-KO mice also expressed significantly (p< 0.0001) increased blood
Mn concentrations with no effect on the concentrations of other metals. (n=5–10) C)
Concentrations of manganese, iron, copper, and zinc in the striatum of *Slc39a14*-KO and
WT male mice. There was a significant increase in striatal Mn concentrations (p=0.0003)
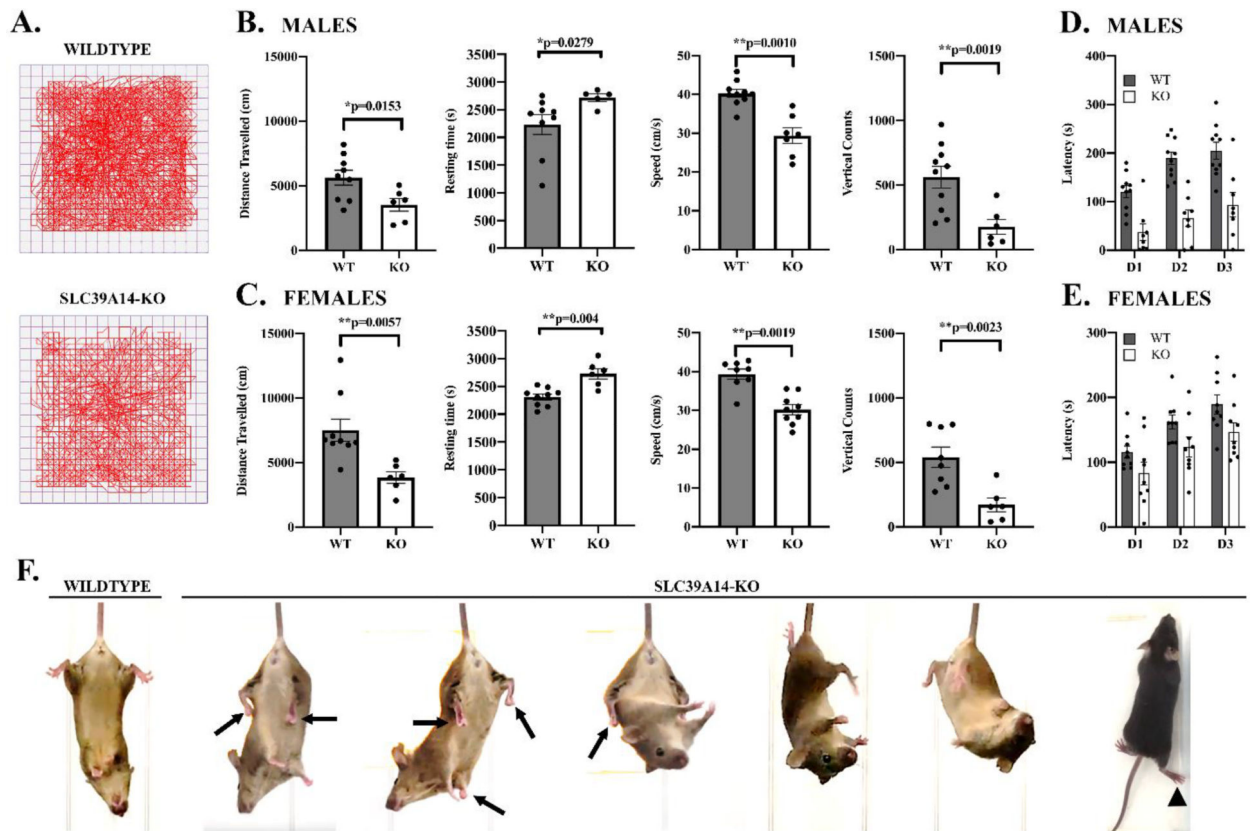
with no effect on other metals. (n=4–5) D) A similar increase (p=0.0012) was measured in the concentration of Mn in the striatum of female mice with no effect on other metals. (n=5–7) Values are mean ± SEM.

Fig. 2: Behavioral assessment of WT and *Slc39a14*-KO PN60 mice:
A) Representative examples of activity cage tracking of the movement of WT and KO mice. B) Analysis of locomotor behavior using activity cages in WT and *Slc39a14*-KO male mice at PN60. There were highly significant effects on the *Slc39a14*-KO mice on distance traveled (decreased, p=0.0153), resting time (increased, p=0.0279), speed (decreased, p = 0.001), and vertical counts (decreased, p= 0.0019). (n=5–9) C) Locomotor behavior of WT and *Slc39a14*-KO female mice. Similar to the male mice, female *Slc39a14*-KO mice also expressed a decrease in distance traveled (p=0.0057), increase in resting time (p= 0004), decrease in speed (p=0.0019), and decrease in vertical counts (p=0.0023). (n=6–9) D) Rotarod performance of WT and *Slc39a14*-KO male mice shows a significant genotype effect $[F_{1,12} = 14.7; p = 0.0001]$ indicating that in *Slc39a14*-KO, the latency to fall from the rotating cylinder was significantly shorter than WT mice. (n=6–10) E) Rotarod performance of WT and *Slc39a14*-KO female mice also show a significant genotype effect $[F_{1,16} = 5.08; p=0.0398 (n=9)]$. F) Observational studies of dystonia features in *Slc39a14*-KO mice using a tail suspension test. We observed dystonia-like movements in the *Slc39a14*-KO mice including trunk twisting, hindlimb clasping, and dragging of the foot while forward walking. Also, we observed backward walking behavior of *Slc39a14*-KO mice at PN21 (see Supplementary Movie 1). Values are mean ± SEM.
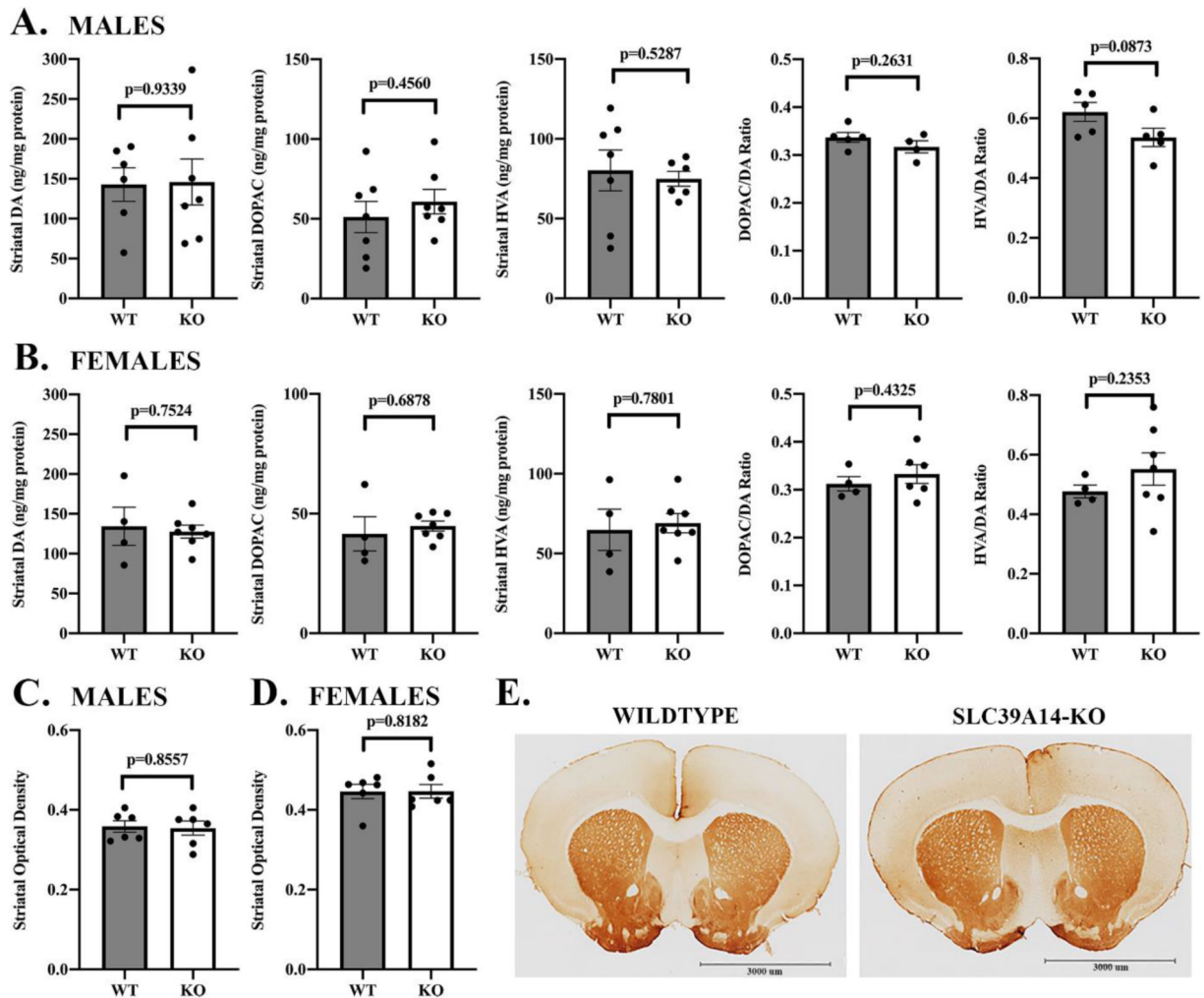
Fig. 3: Analysis of the nigrostriatal dopaminergic system in WT and *Slc39a14*-KO PN60 mice in the corpus striatum:

(A,B) HPLC-electrochemical detection of DA, DOPAC, HVA, DOPAC/DA, and HVA/DA in the striatum of PN60 WT and *Slc39a14*-KO male (A) and (B) female mice. No significant differences were found in any of the measurements in either sex. (n=4–7) (C,D) Tyrosine hydroxylase (TH) immunostaining optical density in the striatum of male (C) and female (D) WT and *Slc39a14*-KO mice. (n=6) E) representative images of TH immunohistochemistry in the striatum of WT and *Slc39a14*-KO mice. No significant differences were found in any of the measurements in either sex. Values are mean ± SEM.
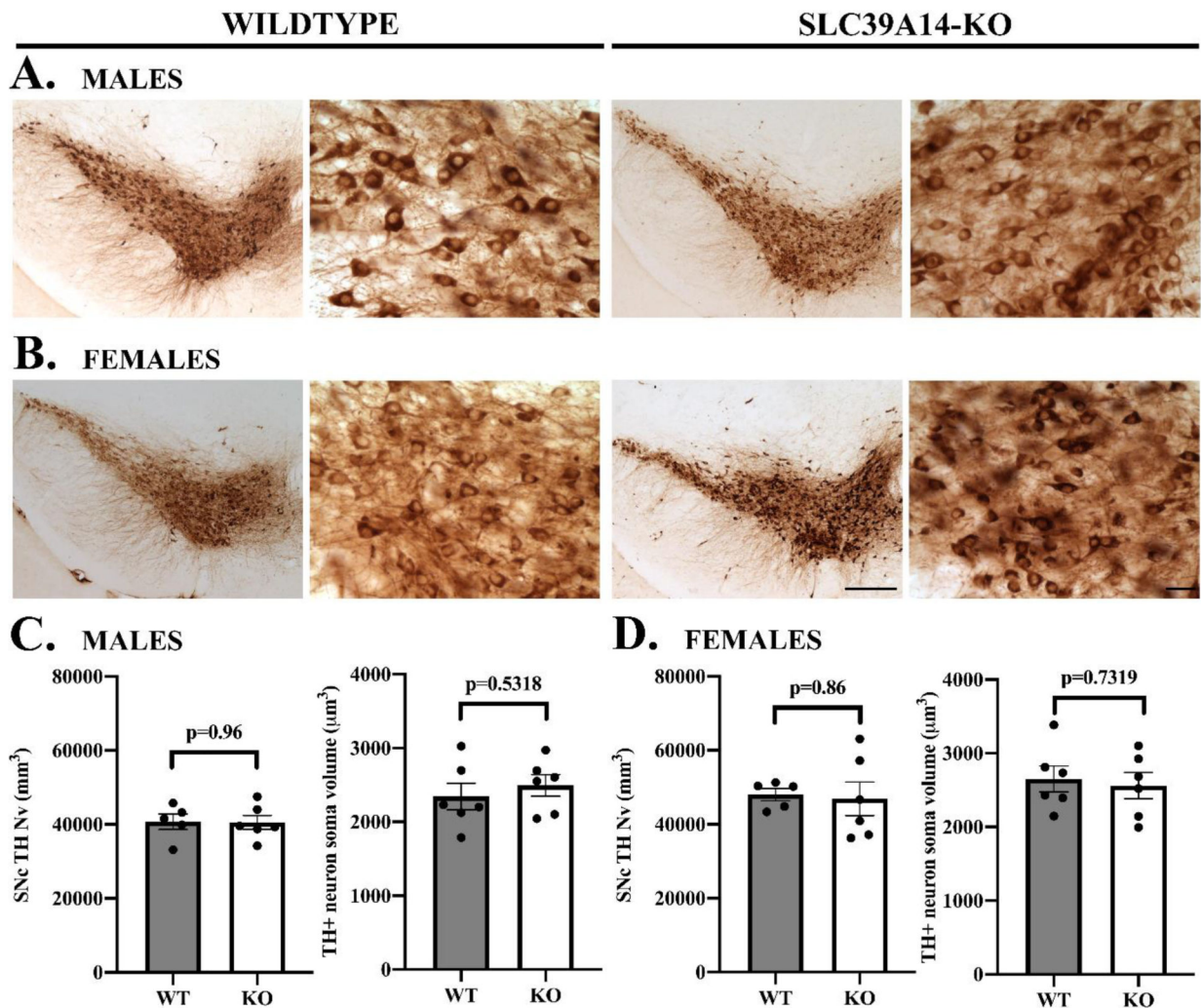
Fig. 4: Unbiased stereological counting of TH-positive dopaminergic neuron density (Nv) and soma volume (SV) in the substantia nigra pars compacta of WT and *Slc39a14*-KO PN60 mice: Photomicrographs of TH immunoreactivity in the SNc of PN60 male (A) and female (B) WT and KO mice. Scale bars = 250 μm (low magnification) or 25 μm (high magnification). There were no significant differences in neuron density (Nv) or soma volume (SV) in the *Slc39a14*-KO male (C) or female (D) mice relative to WT. The average SNc TH-Nv was 40,324/mm^3 in male WT mice (n = 5), 40,561/mm^3 in male *Slc39a14*-KO mice (n = 6), 48,012/mm^3 in female WT mice (n = 5), and 46,913/mm^3 in female *Slc39a14*-KO mice (n = 6). Importantly, SNc TH Nv did not differ between male (t_{10} = 0.06, R^2 = 0.00, p=0.96) or female (t_{10} = 0.21, R^2 = 0.00, p=0.84) WT and *Slc39a14*-KO mice. Values are mean ± SEM.
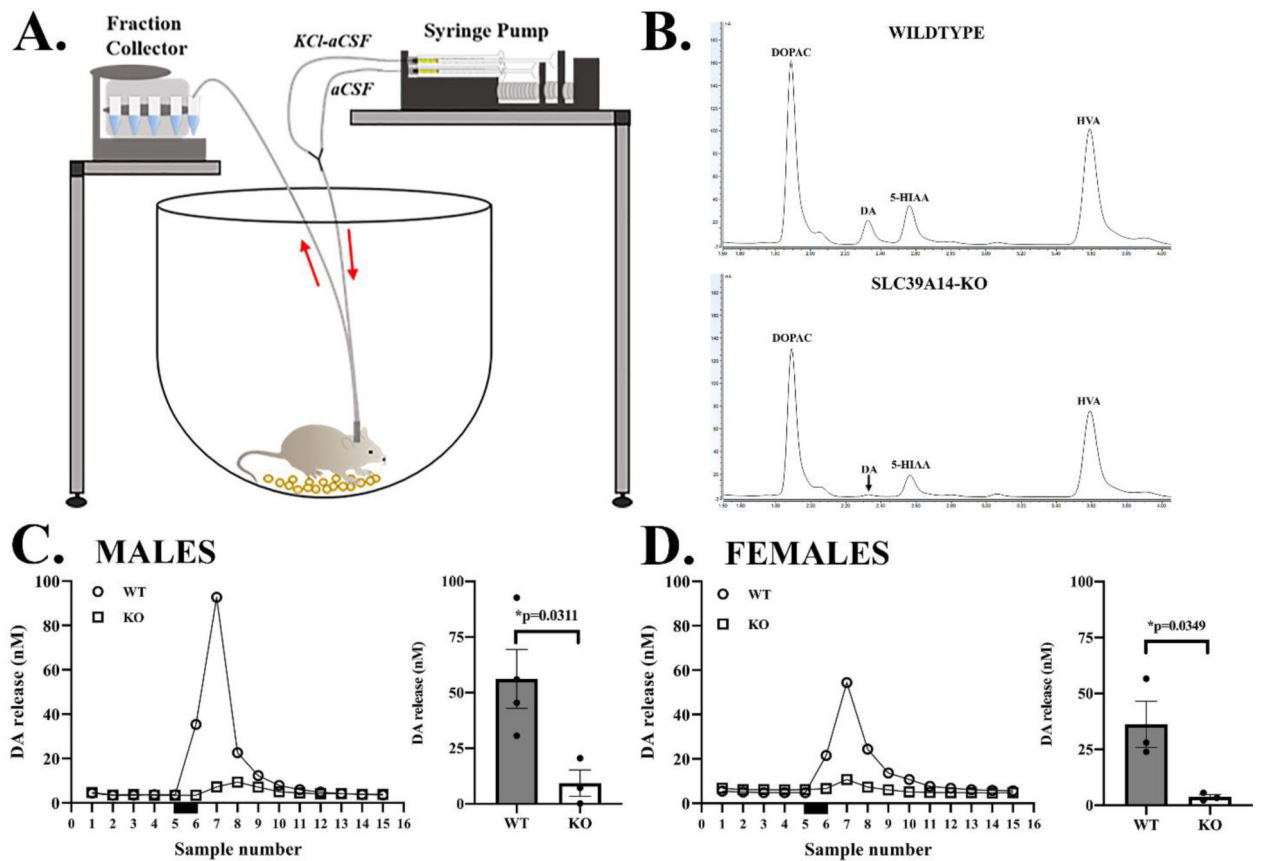
Fig. 5: Analysis of *in vivo* basal and potassium-stimulated dopamine release in the striatum:
We performed analysis of brain dialysate DA concentrations using *in vivo* microdialysis
to assess extracellular basal and potassium-stimulated DA release in the striatum. For
these studies, (A) one WT and *Slc39a14*-KO mice of the same age and sex were
paired and microdialysis performed at the same time with the same solution using a
T split to perfuse each animal's brain and dialysates from each animal was collected
and were immediately analyzed using an HPLC with electrochemical detection. (B)
Representative HPLC-electrochemical chromatogram from a WT and *Slc39a14*-KO mice.
(C) Representative basal and potassium-stimulated DA levels in dialysates as a function of
time in WT and *Slc39a14*-KO male mice. Quantification of results in provided in the graph
to the right of DA release graph. (n=3–4) (D) Representative basal and potassium-stimulated
DA levels in dialysates as a function of time in WT and *Slc39a14*-KO female mice. Black
bar between sample numbers 5 and 6 was the beginning and ending of potassium infusion.
Quantification of results in provided in the graph to the right of DA release graph. (n=3)
Values are mean ± SEM.